Mixing state of black carbon at different atmospheres in north and southwest China

Gang Zhao[1], Tianyi Tan[1], Shuya Hu[1], Zhuofei Du[1], Dongjie Shang[1], Zhijun Wu[1,2], Song Guo[1,2], Jing Zheng[1], Wenfei Zhu[1], Mengren Li[1], Limin Zeng[1,2], Min Hu[1, 2*]

1 State Key Joint Laboratory of Environmental Simulation and Pollution Control, International Joint Laboratory for Regional Pollution Control, Ministry of Education, College of Environmental Sciences and Engineering, Peking University, Beijing, 100871, China

2 Collaborative Innovation Center of Atmospheric Environment and Equipment Technology, Nanjing University of Information Science & Technology, Nanjing, China

[*]**Correspondence author:** Min Hu (minhu@pku.edu.cn)

Abstract

Large uncertainties remain when estimating the radiative forcing by black carbon (BC) because the corresponding microphysical properties have not been well addressed. In this study, the BC size distributions were studied based on three different field campaigns at an urban site, a suburban site, and a background site in China using a single particle soot photometer (SP2) in tandem with a differential mobility diameter. Measurement results indicate that the BC particles were composed of either thinly or thickly coated aerosols. The mean number fractions of the thinly coated BC aerosols were 51%, 67%, and 21% for the urban, suburban, and background sites, respectively. The corresponding thickly coated (thinly coated) core mass median diameters were

187 nm (154 nm), 182 nm (146 nm), and 238 nm (163 nm), respectively. The mean diameter of the thickly coated BC-containing aerosols was larger than that of the thinly coated BC-containing aerosols, while the mean BC core diameter of the thickly coated BC-containing aerosols was smaller than that of the thinly coated BC-containing aerosols. About 10% of the BC-containing aerosols with the BC core are attached to the other non-BC components, which were mainly generated by coagulation between the BC and non-BC components. The measurement results in our study can be further used in modeling studies to help with constraining the uncertainties of the BC radiative effects.

Introduction

Black carbon (BC) plays an important role in the climate system by absorbing solar radiation (Ramanathan and Carmichael, 2008), interacting with the cloud (Roberts et al., 2008), and changing the albedo of the snow (Menon et al., 2002). It is the second most important aerosol component after carbon dioxide, contributing to global warming (Bond et al., 2013). The solar absorption of BC has a significant influence on the development of the boundary layer and then aggravates the air pollution (Ding et al., 2016). The turbulence in the atmospheric boundary layer can be suppressed due to the existence of BC (Wilcox et al., 2016). The BC also plays a remarkable role in driving the formation and trend of regional haze (Zhang et al., 2020).

BC is mainly generated by the incomplete combustion of biofuels and fossil fuels (Bond and Bergstrom, 2006). After emission, the morphology of BC transforms from fractal to spherical and subsequently grows to a fully compact particle with other chemical components coating it (Peng et al., 2016). During the aging process, the BC optical properties change significantly up to a factor of 3 and then the corresponding

magnitude of climate forcing contributed by BC is increased by up to a factor of 2 (Zhang et al., 2008). Large uncertainties remain in estimating the BC radiative effects due to the large variation in BC microphysical properties, such as size distributions and mixing states during the aging process (Zhao et al., 2019; Moffet et al., 2016; Matsui et al., 2018). Therefore, characterizing the differences in size distributions and mixing states between the thinly and thickly coated BC particles can help better constrain the uncertainties of BC aerosol radiative effects. To our best understanding, few studies have specified the mixing states and size distributions of both the thinly and thickly coated BC aerosols.

The thickly coated BC particles can also be classified into two morphological types: bare BC on the surface of non-BC particles or partially coated by non-BC particles (attached type) and BC embedded within or coated by non-BC components (coated type). With the same amount of non-BC components, the mass absorption cross-sections of BC by the attached type are much smaller than those by the coated type (Moteki and Kondo, 2008; Moteki and Kondo, 2010; Moteki et al., 2014). Therefore, the impact of BC on climate can be better estimated when accurately identifying the two types of ambient BC-containing particles. Observations are required to constrain the spatial and temporal microphysical properties of the atmospheric BC.

The single-particle soot photometer (SP2) is always used to measure the mixing states and size distributions of ambient BC particles. In the previous study, advanced technology was used to study the coating over different BC core size diameters on the ground (Liu et al., 2019a) and for vertical profiles (Ding et al., 2019). The measured signals from SP2 can be used to distinguish the BC-containing aerosols as thinly and thickly coated ones. The measured results can also be employed to distinguish the

BC-containing particles between attached and coated types, which were described in detail in the methodology part.

In this study, the tandem SP2 and differential mobility analyzer (DMA) was employed at an urban site, a suburban site, and a background site in China to investigate the microphysical properties of the BC particles. The size distributions and mixing states of both the thinly coated and thickly coated BC aerosols at different atmospheres were characterized. We also investigated the corresponding morphology properties of the BC-containing aerosols. The measured microphysical properties provide the basis for future modeling studies of the BC radiative effects in different environments in China.

2 Methodology

2.1 Measurement sites

The measurements were conducted at three different atmospheric sites in China, namely the urban site of Peking University Urban Atmosphere Environment Monitoring Station (PKU, 39.9°N,116.1°E, 58m a.s.l) in Beijing between 20 January and 4 February 2016, the suburban site of Changping (CP, 40.3°N,116.2°E, 70m a.s.l)) in Beijing between 15 May and 5 June 2016, and the background site of Lijiang (LJ, 27.2°N,100.2°E, 3410 m a.s.l) in Yunnan Province between 22 March and 4 April 2015. The PKU site is located northwest of Beijing. This site could characterize the air pollution of urban Beijing (Hu et al., 2017; Hu et al., 2021b). The CP site locates in the northwest of the Beijing urban area, representing a regional atmosphere (Zhao et al., 2021; Wang et al., 2019b). The LJ site represents the background areas, located in the Mountain Yulong, in the Yunan Province of China (Shang et al., 2018; Zheng et al., 2017; Wang et al., 2019a). The aerosol optical depth at the wavelength of 550 nm

during the year 2020 indicated that the LJ site was very clean and the PKU and CP sites were more polluted as shown in Fig. S1 in the supplement.

2.2 Instruments

2.2.1 DMA-SP2 system

As for the SP2, the continuous Nd: YAG laser beam with the wavelength of 1064 nm is generated intensively in the instrument chamber. When the BC-containing particles pass through the laser beam, they absorb the radiation and then are heated to around 3500-5000 K. The intensity of the emitted incandescent light from the heated BC particle is then transformed to the BC mass concentration. The scattering signals of the BC particle are recorded to estimate the BC particle mixing state.

In this study, the SP2 (Droplet Measurement Technology, Inc., USA) was placed after the DMA (Model 3081, TSI, USA) to measure the size-resolved BC mixing states, and the instrument setup is schematically shown in Fig. S2. The DMA was set to scan the aerosol over the size range between 12.3 and 697 nm every five minutes. The flow rate leading to the SP2 and the condensation particle counter (CPC, Model 3776, TSI, USA) were 0.12 and 0.28 L/min, respectively. The sheath flow of the DMA was 4 L/min.

The Aquadag was used to calibrate the measured incandescence signal of the SP2 using the DMA-SP2 system. The formula from Gysel et al. (2011) was used to convert the mobility diameter into the mass of Aquadag. A correction factor of 0.75 was applied to account for the different response sensitivity of SP2 to Aquadag and ambient BC (Moteki et al., 2010).

In this study, the coating thickness of the BC-containing aerosols was calculated by the difference between the total mobility diameter measured by the DMA and the optical equivalent diameters of the BC core. Details of calculating the optical equivalent coating thickness can refer to Zhang et al. (2018b) and can be found in section 3 in the supplementary material.

2.2.2 Other instruments

The submicron particles (PM_1) chemical compositions were measured using a high-resolution time-of-flight aerosol mass spectrometer (AMS; Aerodyne Research Inc., Billerica, MA, USA). The data processing software PIKA (version 1.16) was used for data analysis. The positive matrix factorization (PMF) analysis was conducted for the source appointment of the organic aerosols (Ulbrich et al., 2009). More details on the measurement of the aerosol chemical compositions and data processing can be found in Zheng et al. (2017).

The mass concentrations of O_3 were measured using UV absorption (model 49i, Thermo Fischer Inc. USA) with a time resolution of 1 minute. The mass concentrations of NO and NO_2 were measured using the chemiluminescence technique (NO-NO_2-NO_x Analyzer, Model 42i, Thermo Scientific, USA). The mass concentrations of SO_2 were measured using the ultraviolet fluorescence method (SO_2 analyzer, model 43i-TLE , Thermo Scientific, USA). The temperature (T), relative humidity (RH), wind speed (WS), and wind direction (WD) were monitored continuously during these campaigns.

2.3 Methodology

For the BC-containing aerosol, there is a lag between the peak time of the scattering and the incandescence signal (Metcalf et al., 2012). The lag time between

the peak scattering signal and the peak incandescence signal can be employed to describe the coating thickness (Moteki and Kondo, 2007; Schwarz et al., 2006) and further used to distinguish the BC-containing aerosols as thinly and thickly coated ones. The lag-time probability distribution at our measurement sites also shows two modes which will be shown in section 3.2, and thus the lag-time can be used to efficiently distinguish the BC-containing aerosols as thinly and thickly coated ones here. It should be noted that, the time-lag method may not effectively distinguish the BC particles between fresh or aged ones because some BC particles sourced from biomass burning (Schwarz et al., 2008b) and solid fuel burning (Liu et al., 2014; Liu et al., 2019b) initially have thick coating but cannot be grouped into aged BC particles.

For the thickly coated BC particles, the measured scattering and incandescence signal can also be employed to distinguish the BC-containing particles as attached and coated types (Moteki et al., 2014) by calculating the time-dependent scattering cross-sections of BC-containing particles (Moteki and Kondo, 2007). For the coated type, all of the coating material will evaporate and the scattering cross-sections will decrease to zero after passing through the laser beam, while the scattering cross-section of the attached BC-containing aerosol will not decrease to zero (Moteki and Kondo, 2008). The method adopted by Dahlkötter et al. (2014) was employed here to characterize the morphology of the BC-containing aerosols. Details of distinguishing the BC-containing particles as attached and coated types can also refer to section 4 in the supplementary materials.

3 Results and discussions

3.1 Overview of the measurement results in different atmospheres

The time series of the measurement results are shown in Fig. S6, Fig. S7, and Fig. S8 for the PKU, CP, and LJ sites, respectively. For the PKU site, the wind was mainly

168 from the north and the wind speed was low with a mean value of 2.2 m/s. The ambient
169 atmosphere was very dry with a mean RH of 27.6%, with minimum and maximum
170 values of 5.8% and 72.6%, respectively. The temperature in the winter in Beijing had a
171 mean value of 0.8 ºC between -5.9 ºC and 9.2 ºC. The mean mass concentration of
172 $PM_{2.5}$ was 49.3±55.4 μg/m^3. The concentration of SO_2 and NO_x (NO_x=NO + NO_2) had
173 the same trends as $PM_{2.5}$, with mean values of 16.3 ± 11.9 ppb and 68.2 ± 63.4 ppb,
174 respectively. The O_3 concentration is anti-correlated with $PM_{2.5}$. For the suburban site
175 CP, the wind showed obvious diurnal cycles with high-speed west wind during the day
176 and low-speed east wind during the night. The mean wind speed was 2.4±1.6 m/s. The
177 RH during the campaign was 38.8 ± 16.0%, with a maximum value of 80.5%. The
178 temperature during the campaign was 21.8±5.2 ºC with a maximum value of 33.2 ºC.
179 As for the NO_x, the mean concentration was 21.4±17.7 ppb. The mean concentration
180 of SO_2 was 2.89±1.10 ppb. The measured mean O_3 concentration was 54.5±38.8 ppb.
181 The mean $PM_{2.5}$ concentration was 22.6±16.8 μg/m^3, with a maximum value of 71.8
182 μg/m^3. As for the background LJ site, The mean value of the wind speed, RH, and T
183 were 3.13 m/s, 50.23%, and 6.5 ºC, respectively. The mean $PM_{2.5}$ mass concentration
184 was 6.2±5.7 μg/m^3. The mean NO_x and SO_2 concentrations were 0.05 ppb and 0.97
185 ppb respectively.

186 The characteristics of the measurement sites are summarized and shown in Fig. 1.
187 The differences in the temperature and RH among these sites mainly resulted from the
188 that the measurements were conducted in different seasons. The concentrations of SO_2,
189 NO_x, and $PM_{2.5}$ indicated that the urban site PKU was the most polluted. The suburban
190 site CP was slightly polluted and the background LJ was the cleanest.

The air mass back trajectories as shown in Fig. S9 during the measurement at PKU show that the measurement site was mainly influenced by the polluted air from the south and southeast, and the relatively clean air from the northwest. The CP site was mainly influenced by the clean air from the northwest and the polluted air from the southeast. The air mass of the LJ site was mainly from the southwest and west.

3.2 Mixing states of the thinly coated and thickly coated BC-containing aerosols

The measured lag time probability distributions for the PKU, CP, and LJ sites are shown in Fig. 2 (a), (b), and (c), respectively. The lag time had two modes for each measurement site. The BC particles are sorted as thinly or thickly coated BC. A two log-normal distribution was used for the probability distribution of the lag time for BC-containing particles as:

$$\mathrm{PDF}(\Delta t) = \sum_{i=1,2} \frac{A_i}{\sqrt{2\pi}\log(\sigma_{g,i})} exp\left[-\frac{\log(\Delta t)-\log(\Delta t_i)}{2log^2(\sigma_{g,i})}\right],$$

Where Δt is the lag time, A_i, $\sigma_{g,i}$, Δt_i are the scale factor, geometric standard deviation, and geometric mean lag time of mode *i* respectively. The critical lag time that distinguishes the thinly and thickly BC particles was determined by calculating the value when the probability distribution values of mode 1 and mode 2 are equal. In this study, the BC-containing aerosols with a lag time larger than 1.4 μs were classified as thickly coated particles for the LJ site. The other BC-containing aerosols were classified as thinly coated particles. Our critical lag time of 1.4 μs is smaller than the previous studies that distinguished the BC-containing aerosols between thinly coated BC and thickly coated BC with a lag time of 2 μs (Moteki and Kondo, 2007; Metcalf et al., 2012),1.8 μs (Metcalf et al., 2012), and 4.2 μs (Liu et al., 2010), which

was determined by the internal setup up of the SP2. The critical lag time for the PKU and CP sites were 1.3 μs and 1.7 μs, respectively.

For each type of BC-containing aerosols, we calculated the coating thickness probabilities and the results are shown in Fig. 2(d), (e) and (f) for the PKU, CP, and LJ sites, respectively. Results showed that the BC-containing aerosols were mainly composed of thickly coated BC aerosols and thinly coated BC aerosols. The coating thickness for the thinly coated BC-containing aerosol was smaller than that of the thickly coated BC-containing aerosols. However, the coating thickness of the thickly coated BC-containing aerosols spread wider than that of the thinly coated ones.

The number fractions of the thickly coated BC-containing aerosols were significantly different for different atmospheres as shown in Fig. 2 (g), (h), and (i). At the polluted urban site, the number concentration of the thickly coated BC-containing aerosols was comparable to that of the thinly coated BC-containing aerosols with the number fractions of 56% and 44% for the thinly coated and thickly coated BC particles, respectively. The number fraction of the thickly coated BC aerosols at the CP site was 67 %. However, the BC-containing aerosols at the background LJ site were dominated by thickly coated ones with a number fraction of 81%.

The difference in the number fraction of the thickly coated BC particles was synthetically influenced by the ambient pollution levels and the sources of the BC aerosols. The suburban site CP had the largest number fraction of the thinly coated BC particles. The CP site is not far from the urban, and thus the thinly coated BC particles from the traffic contribute a large amount of the total ones. The urban site PKU had a larger number fraction of the thickly coated BC than that of the CP site. This might be resulted from the PKU site being more polluted than the CP site and then the aging processing at the PKU site was faster than that at the CP site. The LJ site is far from

239 the traffic sources. The measured BC particles at the LJ site were mainly from
240 long-range transportation and experienced a long time of aging process than that at the
241 CP and PKU sites. Therefore, the BC-containing aerosols were dominated by the
242 thickly coated ones at the LJ sites.

243 We compared the number fraction of the thickly coated BC at different
244 measurement sites from literature (Ueda et al., 2016; Schwarz et al., 2008a; Wang et
245 al., 2017c; Wang et al., 2017a; Wu et al., 2017; Wang et al., 2017b; Wang et al., 2014;
246 Huang et al., 2012; Metcalf et al., 2012; Wang et al., 2016; Shiraiwa et al., 2007;
247 Mcmeeking et al., 2012; Subramanian et al., 2010; Schwarz et al., 2008b; Saha et al.,
248 2018; Krasowsky et al., 2018; Holder et al., 2014) and the results are shown in Fig. 3.
249 The number fraction values were divided into three different kinds of groups, namely
250 the roadside, urban or suburban, and background. Results from Fig. 3 show that the
251 number fractions at the roadside tend to be the lowest. These sites were close to the
252 traffic sources and the measured BC-containing aerosols were mainly from the traffic.
253 The left part of the green circles corresponds to the relatively clean urban or suburban
254 sites with the number fractions of the thickly coated BC around 30%. However, the
255 number fractions of the relative polluted urban or suburban sites had a larger number
256 fraction of the thickly coated BC around 50%. The number fractions of the thickly
257 coated BC at the background sites were the largest. Therefore, the number fractions of
258 the thickly coated BC-containing aerosols were synthetically influenced by the
259 distance from the primary source and the pollution levels of the ambient atmosphere.
260 The number fraction of the thickly coated BC-containing aerosols increased with the
261 distance from the primary emission sources and the pollution levels. Our results were
262 consistent with the aerial measurement by Metcalf et al. (2012), who found that the
263 number fraction of the thickly coated BC was 29%~41% at the top of the Los Angeles
264 city and 47%-54% for the out plume of this city.

For a better understanding of the source of the thinly coated and thickly coated BC, we compared the number concentrations of the BC-containing aerosols with the source apportionment results from the AMS data for the CP site. Among the PMF results, the factor of hydrocarbon-like organic aerosol (HOA) is mainly composed of long-chain hydrocarbon, and oxygenated organic aerosol (OOA) is mainly from the secondary formation. HOA is mainly from the diesel exhaust, gasoline exhaust, and lubricating oil emission. From Fig. 4(a), the number concentration of the thinly coated BC and mass concentration of HOA showed good consistency, with R^2 equaling 0.69 as shown in Fig. S10, which further proved the evidence that the thinly coated BC-containing aerosols were from the traffic sources. The time series of the thickly coated BC and OOA showed good consistency as shown in Fig. 4 (b), with R^2 equaling 0.87. Therefore, the aging processing of the ambient BC was accompanied by the ambient OA. The mass concentration of OOA and the number concentration of thickly coated BC can be used as good indicators for each other.

3.3 Size distributions of the thinly coated and thickly coated BC-containing aerosols

The size distributions of the BC-containing aerosols exert a significant influence on their corresponding radiative effects (Zhao et al., 2019; Matsui et al., 2018). We calculated the number size distribution (NSD) of BC-containing aerosols for the thinly coated and thickly coated ones at different sites, and the results are shown in Fig. 5. It should be noted that the Dp in Fig. 5 corresponds to the mobility diameter from the DMA. The BC-containing aerosol NSD was further fit using the log-normal distribution.

As for the thinly coated BC-containing aerosols, the geometric mean diameters were 193, 161, and 162 nm for the PKU, CP, and LJ sites, respectively. The geometric

290 standard deviations (GSD) of the BC-containing aerosol NSD were 1.50, 1.63, and
291 1.91 for the PKU, CP, and LJ sites, respectively. The GSD to some extent reflects the
292 diversity of the BC sources. The LJ site had the largest GSD, which indicated multiple
293 sources of thinly coated BC-containing aerosols. The LJ site was highly influenced by
294 atmospheric transportation, due to the high altitude of this location (Zheng et al., 2017;
295 Tan et al., 2021). Therefore, the thinly coated BC-containing aerosols could be
296 originated from different orientations. As for the urban site PKU, the thinly coated BC
297 aerosols were mainly from urban lifestyle emissions. Therefore, the thinly coated BC
298 aerosols at the PKU site had the lowest value of the GSD. However, the thinly coated
299 BC aerosols at the suburban site CP were influenced synthetically by urban lifestyle
300 sources and some other sources from suburban, and thus had a larger value of GSD
301 than that of PKU.

302 As for the thickly coated BC, it is obvious that they had larger diameters than those
303 of the thinly coated BC due to the coating of other non-BC components. The
304 geometric mean Dp values of the thickly coated BC were 294, 244, and 257 nm for the
305 PKU, CP, and LJ sites, respectively. The corresponding GSD values were 1.37, 1.41,
306 and 1.46.

307 Based on the above results, the geometric mean Dp values of the thickly coated
308 BC aerosols were larger than that of the thinly coated BC aerosols by 52%, 52%, and
309 59% for the PKU, CP, and LJ sites, respectively. The GSD values of the thickly coated
310 BC were consistent with that of the thinly coated BC with the lowest value at the PKU
311 site and highest value at the LJ site, which is consistent with the diversity of the
312 sources of BC-containing aerosols. For each site, the GSD values of the thickly coated
313 BC aerosols were smaller than that of the thinly coated ones. The GSD of
314 BC-containing aerosols tends to be smaller during the aging processing because the

315 increment of the diameter should decrease with the diameter.

316 **3.4 Size distribution of the thinly coated and thickly coated BC core**

317 The number and mass concentrations of the BC core under different mass
318 equivalent diameters were calculated and the results are shown in Fig. 6 and Table 1.
319 It should be noted here that, when it comes to the BC size distribution, the
320 mass-equivalent diameter of BC cores (D_{me}) (assuming a density of 1.8 g/cm^3) was
321 adopted in this study for direct comparison with previous studies.

322 As for the number size distribution of the BC core, the geometric mean D_{me} of
323 the thinly coated BC particles were 115, 107, and 127 nm, for the PKU, CP, and LJ
324 sites respectively. The corresponding GSD values are 1.58 1.53 and 1.68, respectively.
325 The D_{me} for the thickly coated BC particles were 114, 95, and 111 nm for the PKU,
326 CP, and LJ sites respectively and the corresponding GSD values were 1.40, 1.45, and
327 1.43, respectively. Both the GSD and the D_{me} of the thickly coated BC were smaller
328 than that of the thinly coated BC. The overall geometric mean diameter of the BC core
329 number size distributions are 114, 100, and 111 nm for the PKU, CP, and LJ sites
330 respectively.

331 There are mainly three possible reasons that may lead to the rather smaller
332 geometric mean diameter for the thinly coated BC than the thickly coated BC. First,
333 the smaller BC core tends to have a higher time lag as a smaller BC core will take a
334 longer time to evaporate the coating on it and thus the thinly coated particles tend to
335 have smaller core diameters. Second, it takes less time for the smaller BC particles to
336 grow the same amount of coating thickness when the increment of the BC particles
337 was dominated by condensation Thirdly, the small BC particles may have a longer life
338 than the large BC particles.

As for the mass size distribution of the BC core, the geometric mean D_{me} of the thinly coated BC were 187, 182, and 238 nm for the PKU, CP, and LJ sites respectively and the corresponding GSD values were 1.35, 1.48, and 1.47. The overall geometric mean diameter of the BC core mass distributions are 172, 169, and 181 nm for the PKU, CP, and LJ sites respectively. The geometric mean diameter of the BC core mass distributions of 172 nm in PKU was slightly smaller than that of Liu et al. (2019a), with a geometric mean diameter of 195 nm in another measurement in the urban environment in Beijing and comparable to Zhang et al. (2018a) with a geometric mean diameter of the BC core around 180 nm.

3.5 Morphology of the BC-containing aerosols

The time series of the number fractions of the attached BC-containing aerosols to the total BC- containing aerosols ($f_{attached}$) are shown in Fig. 7. From Fig. 7, the $f_{attached}$ ranged between 0 and 0.21 with a mean value of 7.2 ± 3.7%, 11.0 ± 3.7%, and 10.1 ± 4.1%. Moteki et al. (2014) found that the $f_{attached}$ was generally less than 0.1 in Tokyo. The $f_{attached}$ ranged between 3% and 16% in suburban London (Liu et al., 2015). A mean value of 12% was found for biomass burning particles using electron microscopy (China et al., 2013). Our measurement results were consistent with the previous studies. The $f_{attached}$ tend to increase with the $PM_{2.5}$ for different sites, which may indicate that the attached BC-containing aerosols were generated from the coagulation of BC and non-BC aerosols.

We calculated the $f_{attached}$ under different aerosol diameters and the results are shown in Fig. 8. There were few attached BC-containing aerosols when the diameter was smaller than 250 nm with $f_{attached}$ lowing than 2%. The $f_{attached}$ increased with the diameter for all of the measurement sites. It could reach 30% for the LJ sites. Based on the results from the electron microscopy, the BC volume fractions are smaller than

those of the non-BC volume fractions in the attached BC aerosols (Moteki et al., 2014). The increment of $f_{attached}$ with Dp is essentially consistent with the results from Hu et al. (2021a) that larger Dp contains more fractal BC, which is hard to be enveloped by coatings. Our results further indicate that the attached BC aerosols were formed from coagulation, as the coagulation efficiency of the two particles increased with the difference between their sizes (Cai and Jiang, 2017; Kim et al., 2016; Mahfouz and Donahue, 2021).

Under the heavier pollution, more secondary aerosol forms and more condensation process would on one hand increase the coating of the previously coated BC particles, which would not increase the number fraction of coated BC. On the other hand, the condensation process would coat on the attached BC particle and to some content would lead to the transformation from the attached BC to coated BC particles. Based on our measurement results, the above process of transformation from attached BC to coated BC may not be comparable to the process of coagulation between thinly coated BC and non-BC particles, which would lead to the increment of the fraction of attached BC with the pollution levels.

The $f_{attached}$ under different aerosol number concentrations (N) and different ratios of the BC-free aerosol number concentrations to the BC-containing aerosol number concentrations are shown in Fig. 9. Results showed that the $f_{attached}$ increased with the above two factors. The results were consistent with the fact that the coagulation between BC and non-BC components is more likely to happen with the increment of the BC-free aerosol number concentrations. Based on the analysis above, we concluded that the attached BC- containing aerosols are mainly formed through coagulation.

4 Conclusions

In this study, the BC microphysical properties were studied based on field measurement using the DMA-SP2 system at the urban site PKU, suburban site CP and a background site LJ in China.

The number fractions of the thickly coated BC-containing aerosols were 49%, 33%, and 79% for the PKU, CP, and LJ sites respectively. The mass concentrations of the thinly coated BC-containing aerosols showed good consistency with that of HOA, which indicated that the thinly coated BC-containing aerosols were mainly generated from the emission of vehicles. The thickly coated BC-containing aerosols are highly correlated with the OOA.

The geometric diameter of the thinly coated BC-containing aerosols ranged between 160 nm and 200 nm, while the corresponding range was 240~300 nm for the thickly coated BC-containing aerosols. The GSD of the BC-containing aerosols decreased during the aging process. The corresponding mobility diameters of these thickly coated (thinly coated) BC-containing aerosols were 294 (193), 244 (161), and 257 (162) nm. The measured thickly coated (thinly coated) BC core number median diameters were 115 (114), 107 (95), and 127 (111) nm for the urban, suburban, and background sites, respectively. The corresponding thickly coated (thinly coated) core mass median diameters were 187 (154), 182 (146), and 238 (163) nm respectively. The mean diameter of the thickly coated BC-containing aerosols was larger than that of the thinly coated BC-containing aerosols, while the mean BC core diameter of the thickly coated BC-containing aerosols was smaller than that of the thinly coated BC-containing aerosols. There are about 10% of the BC-containing aerosols with the BC core attached to the other non-BC components. We concluded that these attached BC-containing aerosols were mainly generated by coagulation between the BC and non-BC components even though the aging of the ambient BC aerosols was driven by condensation.

Data availability. The data is available at https://doi.org/10.5281/zenodo.5816310.

Author contributions. **Gang Zhao:** Conceptualization, Writing - Original Draft, Visualization, Software, **Tianyi Tan:** Data Curation, Conceptualization, Visualization, **Shuya Hu**: Data Curation, Conceptualization, **Zhuofei Du:** Data Curation, **Dongjie Shang:** Data Curation, **Zhijun Wu**: Data Curation, Conceptualization, **Song Guo**: Data Curation, Conceptualization**, Jing Zheng**: Data Curation, Conceptualization**, Wenfei Zhu**: Data Curation, Conceptualization**, Mengren Li**: Data Curation, Conceptualization**, Limin Zeng**: Data Curation, Conceptualization**, Min Hu**: Resources, Supervision, Data Curation, Conceptualization, Revision.

Competing interests. The authors declare that they have no conflict of interest.

Acknowledgments. This work is supported by the China Postdoctoral Science Foundation (2021M700192) and the National Natural Science Foundation of China (91844301).

References

Bond, T. C. and Bergstrom, R. W.: Light Absorption by Carbonaceous Particles: An Investigative Review, Aerosol Sci. Technol., 40, 27-67, 10.1080/02786820500421521, 2006.

Bond, T. C., Doherty, S. J., Fahey, D. W., Forster, P. M., Berntsen, T., DeAngelo, B. J., Flanner, M. G., Ghan, S., Karcher, B., Koch, D., Kinne, S., Kondo, Y., Quinn, P. K., Sarofim, M. C., Schultz, M. G., Schulz, M., Venkataraman, C., Zhang, H., Zhang, S., Bellouin, N., Guttikunda, S. K., Hopke, P. K., Jacobson, M. Z., Kaiser, J. W., Klimont, Z., Lohmann, U., Schwarz, J. P., Shindell, D., Storelvmo, T., Warren, S. G., and

Zender, C. S.: Bounding the role of black carbon in the climate system: A scientific assessment, J Geophys Res-Atmos, 118, 5380-5552, 10.1002/jgrd.50171, 2013.

Cai, R. and Jiang, J.: A new balance formula to estimate new particle formation rate: reevaluating the effect of coagulation scavenging, Atmospheric Chemistry and Physics, 17, 12659-12675, 10.5194/acp-17-12659-2017, 2017.

China, S., Mazzoleni, C., Gorkowski, K., Aiken, A. C., and Dubey, M. K.: Morphology and mixing state of individual freshly emitted wildfire carbonaceous particles, Nature communications, 4, 2122, 10.1038/ncomms3122, 2013.

Dahlkötter, F., Gysel, M., Sauer, D., Minikin, A., Baumann, R., Seifert, P., Ansmann, A., Fromm, M., Voigt, C., and Weinzierl, B.: The Pagami Creek smoke plume after long-range transport to the upper troposphere over Europe – aerosol properties and black carbon mixing state, Atmospheric Chemistry and Physics, 14, 6111-6137, 10.5194/acp-14-6111-2014, 2014.

Ding, A., Huang, X., Nie, W., Sun, J., Kerminen, V.-M., Petäjä, T., Su, H., Cheng, Y., Yang, X.-Q., Wang, M., Chi, X., Wang, J., Virkkula, A., Guo, W., Yuan, J., Wang, S. R., Zhang, R., Wu, Y., Song, Y. C., Zhu, T., Zilitinkevich, S., Kulmala, M., and Fu, C.: Enhanced haze pollution by black carbon in megacities in China, Geophys. Res. Lett., 43, 2873-2879, 2016.

Ding, S., Liu, D., Zhao, D., Hu, K., Tian, P., Zhou, W., Huang, M., Yang, Y., Wang, F., Sheng, J., Liu, Q., Kong, S., Cui, P., Huang, Y., He, H., Coe, H., and Ding, D.: Size-Related Physical Properties of Black Carbon in the Lower Atmosphere over Beijing and Europe, Environ Sci Technol, 53, 11112-11121, 10.1021/acs.est.9b03722, 2019.

Gysel, M., Laborde, M., Olfert, J. S., Subramanian, R., and Gröhn, A. J.: Effective density of Aquadag and fullerene soot black carbon reference materials used for SP2 calibration, Atmospheric Measurement Techniques, 4, 2851-2858, 10.5194/amt-4-2851-2011, 2011.

Holder, A. L., Hagler, G. S. W., Yelverton, T. L. B., and Hays, M. D.: On-road black carbon instrument intercomparison and aerosol characteristics by driving environment, Atmospheric Environment, 88, 183-191, https://doi.org/10.1016/j.atmosenv.2014.01.021, 2014.

Hu, K., Liu, D., Tian, P., Wu, Y., Deng, Z., Wu, Y., Zhao, D., Li, R., Sheng, J., Huang, M., Ding, D., Li, W., Wang, Y., and Wu, Y.: Measurements of the Diversity of Shape and Mixing State for Ambient Black Carbon Particles, Geophys. Res. Lett., 48, 10.1029/2021gl094522, 2021a.

Hu, S., Zhao, G., Tan, T., Li, C., Zong, T., Xu, N., Zhu, W., and Hu, M.: Current challenges of improving visibility due to increasing nitrate fraction in PM2.5 during the haze days in Beijing, China, Environmental Pollution, 290, 118032, 10.1016/j.envpol.2021.118032, 2021b.

Hu, W., Hu, M., Hu, W.-W., Zheng, J., Chen, C., Wu, Y., and Guo, S.: Seasonal variations in high time-resolved chemical compositions, sources, and evolution of atmospheric submicron aerosols in the megacity Beijing, Atmospheric Chemistry and Physics, 17, 9979-10000, 10.5194/acp-17-9979-2017, 2017.

Huang, X.-F., Sun, T.-L., Zeng, L.-W., Yu, G.-H., and Luan, S.-J.: Black carbon aerosol characterization in a coastal city in South China using a single particle soot photometer, Atmospheric Environment, 51, 21-28, https://doi.org/10.1016/j.atmosenv.2012.01.056, 2012.

Kim, Y.-h., Yiacoumi, S., Nenes, A., and Tsouris, C.: Charging and coagulation of radioactive and nonradioactive particles in the atmosphere, Atmospheric Chemistry and Physics, 16, 3449-3462, 10.5194/acp-16-3449-2016, 2016.

Krasowsky, T. S., McMeeking, G. R., Sioutas, C., and Ban-Weiss, G.: Characterizing the evolution of physical properties and mixing state of black carbon particles: from near a major highway to the broader urban plume in Los Angeles, Atmos. Chem. Phys., 18, 11991-12010, 10.5194/acp-18-11991-2018, 2018.

492 Liu, D., Allan, J. D., Young, D. E., Coe, H., Beddows, D., Fleming, Z. L., Flynn, M. J.,
493 Gallagher, M. W., Harrison, R. M., Lee, J., Prevot, A. S. H., Taylor, J. W., Yin, J.,
494 Williams, P. I., and Zotter, P.: Size distribution, mixing state and source
495 apportionment of black carbon aerosol in London during wintertime, Atmospheric
496 Chemistry and Physics, 14, 10061-10084, 10.5194/acp-14-10061-2014, 2014.
497 Liu, D., Joshi, R., Wang, J., Yu, C., Allan, J. D., Coe, H., Flynn, M. J., Xie, C., Lee, J.,
498 Squires, F., Kotthaus, S., Grimmond, S., Ge, X., Sun, Y., and Fu, P.: Contrasting
499 physical properties of black carbon in urban Beijing between winter and summer,
500 Atmospheric Chemistry and Physics, 19, 6749-6769, 10.5194/acp-19-6749-2019,
501 2019a.
502 Liu, D., Flynn, M., Gysel, M., Targino, A., Crawford, I., Bower, K., Choularton, T.,
503 Jurányi, Z., Steinbacher, M., Hüglin, C., Curtius, J., Kampus, M., Petzold, A.,
504 Weingartner, E., Baltensperger, U., and Coe, H.: Single particle characterization of
505 black carbon aerosols at a tropospheric alpine site in Switzerland, Atmospheric
506 Chemistry and Physics, 10, 7389-7407, 10.5194/acp-10-7389-2010, 2010.
507 Liu, H., Pan, X., Liu, D., Liu, X., Chen, X., Tian, Y., Sun, Y., Fu, P., and Wang, Z.:
508 Mixing characteristics of refractory black carbon aerosols determined by a tandem
509 CPMA-SP2 system at an urban site in Beijing, Atmospheric Chemistry and Physics
510 Discussions, 1-25, 10.5194/acp-2019-244, 2019b.
511 Liu, S., Aiken, A. C., Gorkowski, K., Dubey, M. K., Cappa, C. D., Williams, L. R.,
512 Herndon, S. C., Massoli, P., Fortner, E. C., Chhabra, P. S., Brooks, W. A., Onasch, T.
513 B., Jayne, J. T., Worsnop, D. R., China, S., Sharma, N., Mazzoleni, C., Xu, L., Ng, N.
514 L., Liu, D., Allan, J. D., Lee, J. D., Fleming, Z. L., Mohr, C., Zotter, P., Szidat, S., and
515 Prevot, A. S.: Enhanced light absorption by mixed source black and brown carbon
516 particles in UK winter, Nature communications, 6, 8435, 10.1038/ncomms9435, 2015.

517 Mahfouz, N. G. A. and Donahue, N. M.: Technical note: The enhancement limit of
518 coagulation scavenging of small charged particles, Atmos. Chem. Phys., 21,
519 3827-3832, 10.5194/acp-21-3827-2021, 2021.
520 Matsui, H., Hamilton, D. S., and Mahowald, N. M.: Black carbon radiative effects
521 highly sensitive to emitted particle size when resolving mixing-state diversity, Nature
522 communications, 9, 3446, 10.1038/s41467-018-05635-1, 2018.
523 McMeeking, G. R., Bart, M., Chazette, P., Haywood, J. M., Hopkins, J. R., McQuaid,
524 J. B., Morgan, W. T., Raut, J. C., Ryder, C. L., Savage, N., Turnbull, K., and Coe, H.:
525 Airborne measurements of trace gases and aerosols over the London metropolitan
526 region, Atmos. Chem. Phys., 12, 5163-5187, 10.5194/acp-12-5163-2012, 2012.
527 Menon, S., Hansen, J., Nazarenko, L., and Luo, Y.: Climate effects of black carbon
528 aerosols in China and India, Science, 297, 2250-2253, 10.1126/science.1075159,
529 2002.
530 Metcalf, A. R., Craven, J. S., Ensberg, J. J., Brioude, J., Angevine, W., Sorooshian, A.,
531 Duong, H. T., Jonsson, H. H., Flagan, R. C., and Seinfeld, J. H.: Black carbon aerosol
532 over the Los Angeles Basin during CalNex, Journal of Geophysical Research:
533 Atmospheres, 117, https://doi.org/10.1029/2011JD017255, 2012.
534 Moffet, R. C., amp, apos, Brien, R. E., Alpert, P. A., Kelly, S. T., Pham, D. Q., Gilles,
535 M. K., Knopf, D. A., and Laskin, A.: Morphology and mixing of black carbon
536 particles collected in central California during the CARES field study, Atmospheric
537 Chemistry and Physics, 16, 14515-14525, 10.5194/acp-16-14515-2016, 2016.
538 Moteki, N. and Kondo, Y.: Effects of Mixing State on Black Carbon Measurements by
539 Laser-Induced Incandescence, Aerosol Sci. Technol., 41, 398-417,
540 10.1080/02786820701199728, 2007.
541 Moteki, N. and Kondo, Y.: Method to measure time-dependent scattering cross
542 sections of particles evaporating in a laser beam, Journal of Aerosol Science, 39,
543 348-364, 10.1016/j.jaerosci.2007.12.002, 2008.

544 Moteki, N. and Kondo, Y.: Dependence of Laser-Induced Incandescence on Physical
545 Properties of Black Carbon Aerosols: Measurements and Theoretical Interpretation,
546 Aerosol Sci. Technol., 44, 663-675, Pii 924375405

547 10.1080/02786826.2010.484450, 2010.
548 Moteki, N., Kondo, Y., and Adachi, K.: Identification by single-particle soot
549 photometer of black carbon particles attached to other particles: Laboratory
550 experiments and ground observations in Tokyo, Journal of Geophysical Research:
551 Atmospheres, 119, 1031-1043, https://doi.org/10.1002/2013JD020655, 2014.
552 Moteki, N., Kondo, Y., and Nakamura, S.-i.: Method to measure refractive indices of
553 small nonspherical particles: Application to black carbon particles, Journal of Aerosol
554 Science, 41, 513-521, https://doi.org/10.1016/j.jaerosci.2010.02.013, 2010.
555 Peng, J., Hu, M., Guo, S., Du, Z., Zheng, J., Shang, D., Levy Zamora, M., Zeng, L.,
556 Shao, M., Wu, Y.-S., Zheng, J., Wang, Y., Glen, C. R., Collins, D. R., Molina, M. J.,
557 and Zhang, R.: Markedly enhanced absorption and direct radiative forcing of black
558 carbon under polluted urban environments, Proceedings of the National Academy of
559 Sciences, 201602310, 10.1073/pnas.1602310113, 2016.
560 Ramanathan, V. and Carmichael, G.: Global and regional climate changes due to black
561 carbon, Nature Geoscience, 1, 221-227, 10.1038/ngeo156, 2008.
562 Roberts, G. C., Ramana, M. V., Corrigan, C., Kim, D., and Ramanathan, V.:
563 Simultaneous observations of aerosol-cloud-albedo interactions with three stacked
564 unmanned aerial vehicles, Proceedings of the National Academy of Sciences of the
565 United States of America, 105, 7370-7375, 10.1073/pnas.0710308105, 2008.
566 Saha, P. K., Khlystov, A., and Grieshop, A. P.: Downwind evolution of the volatility
567 and mixing state of near-road aerosols near a US interstate highway, Atmos. Chem.
568 Phys., 18, 2139-2154, 10.5194/acp-18-2139-2018, 2018.

569 Schwarz, J. P., Spackman, J. R., Fahey, D. W., Gao, R. S., Lohmann, U., Stier, P.,
570 Watts, L. A., Thomson, D. S., Lack, D. A., Pfister, L., Mahoney, M. J., Baumgardner,
571 D., Wilson, J. C., and Reeves, J. M.: Coatings and their enhancement of black carbon
572 light absorption in the tropical atmosphere, J Geophys Res-Atmos, 113,
573 10.1029/2007jd009042, 2008a.
574 Schwarz, J. P., Gao, R. S., Spackman, J. R., Watts, L. A., Thomson, D. S., Fahey, D.
575 W., Ryerson, T. B., Peischl, J., Holloway, J. S., Trainer, M., Frost, G. J., Baynard, T.,
576 Lack, D. A., de Gouw, J. A., Warneke, C., and Del Negro, L. A.: Measurement of the
577 mixing state, mass, and optical size of individual black carbon particles in urban and
578 biomass burning emissions, Geophys. Res. Lett., 35,
579 https://doi.org/10.1029/2008GL033968, 2008b.
580 Schwarz, J. P., Gao, R. S., Fahey, D. W., Thomson, D. S., Watts, L. A., Wilson, J. C.,
581 Reeves, J. M., Darbeheshti, M., Baumgardner, D. G., Kok, G. L., Chung, S. H., Schulz,
582 M., Hendricks, J., Lauer, A., Kärcher, B., Slowik, J. G., Rosenlof, K. H., Thompson, T.
583 L., Langford, A. O., Loewenstein, M., and Aikin, K. C.: Single-particle measurements
584 of midlatitude black carbon and light-scattering aerosols from the boundary layer to
585 the lower stratosphere, Journal of Geophysical Research, 111, 10.1029/2006jd007076,
586 2006.
587 Shang, D., Hu, M., Zheng, J., Qin, Y., Du, Z., Li, M., Fang, J., Peng, J., Wu, Y., Lu, S.,
588 and Guo, S.: Particle number size distribution and new particle formation under the
589 influence of biomass burning at a high altitude background site at Mt. Yulong
590 (3410 m), China, Atmospheric Chemistry and Physics, 18, 15687-15703,
591 10.5194/acp-18-15687-2018, 2018.
592 Shiraiwa, M., Kondo, Y., Moteki, N., Takegawa, N., Miyazaki, Y., and Blake, D. R.:
593 Evolution of mixing state of black carbon in polluted air from Tokyo, Geophys. Res.
594 Lett., 34, https://doi.org/10.1029/2007GL029819, 2007.

595 Subramanian, R., Kok, G. L., Baumgardner, D., Clarke, A., Shinozuka, Y., Campos, T.
596 L., Heizer, C. G., Stephens, B. B., de Foy, B., Voss, P. B., and Zaveri, R. A.: Black
597 carbon over Mexico: the effect of atmospheric transport on mixing state, mass
598 absorption cross-section, and BC/CO ratios, Atmos. Chem. Phys., 10, 219-237,
599 10.5194/acp-10-219-2010, 2010.
600 Tan, T., Hu, M., Du, Z., Zhao, G., Shang, D., Zheng, J., Qin, Y., Li, M., Wu, Y., Zeng,
601 L., Guo, S., and Wu, Z.: Measurement report: Strong light absorption induced by aged
602 biomass burning black carbon over the southeastern Tibetan Plateau in pre-monsoon
603 season, Atmospheric Chemistry and Physics, 21, 8499-8510,
604 10.5194/acp-21-8499-2021, 2021.
605 Ueda, S., Nakayama, T., Taketani, F., Adachi, K., Matsuki, A., Iwamoto, Y., Sadanaga,
606 Y., and Matsumi, Y.: Light absorption and morphological properties of
607 soot-containing aerosols observed at an East Asian outflow site, Noto Peninsula, Japan,
608 Atmos. Chem. Phys., 16, 2525-2541, 10.5194/acp-16-2525-2016, 2016.
609 Ulbrich, I. M., Canagaratna, M. R., Zhang, Q., Worsnop, D. R., and Jimenez, J. L.:
610 Interpretation of organic components from Positive Matrix Factorization of aerosol
611 mass spectrometric data, Atmospheric Chemistry and Physics, 9, 2891-2918,
612 10.5194/acp-9-2891-2009, 2009.
613 Wang, J., Zhang, Q., Chen, M., Collier, S., Zhou, S., Ge, X., Xu, J., Shi, J., Xie, C.,
614 Hu, J., Ge, S., Sun, Y., and Coe, H.: First Chemical Characterization of Refractory
615 Black Carbon Aerosols and Associated Coatings over the Tibetan Plateau (4730 m
616 a.s.l), Environmental Science & Technology, 51, 14072-14082,
617 10.1021/acs.est.7b03973, 2017a.
618 Wang, Q., Huang, R. J., Cao, J., Han, Y., Wang, G., Li, G., Wang, Y., Dai, W., Zhang,
619 R., and Zhou, Y.: Mixing State of Black Carbon Aerosol in a Heavily Polluted Urban
620 Area of China: Implications for Light Absorption Enhancement, Aerosol Sci. Technol.,
621 48, 689-697, 10.1080/02786826.2014.917758, 2014.

622 Wang, Q., Huang, R., Zhao, Z., Cao, J., Ni, H., Tie, X., Zhu, C., Shen, Z., Wang, M.,
623 Dai, W., Han, Y., Zhang, N., and Prevot, A. S. H.: Effects of photochemical oxidation
624 on the mixing state and light absorption of black carbon in the urban atmosphere of
625 China, Environmental Research Letters, 12, 10.1088/1748-9326/aa64ea, 2017b.
626 Wang, Q., Huang, R.-J., Zhao, Z., Zhang, N., Wang, Y., Ni, H., Tie, X., Han, Y.,
627 Zhuang, M., Wang, M., Zhang, J., Zhang, X., Dusek, U., and Cao, J.: Size distribution
628 and mixing state of refractory black carbon aerosol from a coastal city in South China,
629 Atmospheric Research, 181, 163-171, https://doi.org/10.1016/j.atmosres.2016.06.022,
630 2016.
631 Wang, Y., Liu, F., He, C., Bi, L., Cheng, T., Wang, Z., Zhang, H., Zhang, X., Shi, Z.,
632 and Li, W.: Fractal Dimensions and Mixing Structures of Soot Particles during
633 Atmospheric Processing, Environmental Science & Technology Letters, 4, 487-493,
634 10.1021/acs.estlett.7b00418, 2017c.
635 Wang, Y., Hu, M., Lin, P., Tan, T., Li, M., Xu, N., Zheng, J., Du, Z., Qin, Y., Wu, Y.,
636 Lu, S., Song, Y., Wu, Z., Guo, S., Zeng, L., Huang, X., and He, L.: Enhancement in
637 Particulate Organic Nitrogen and Light Absorption of Humic-Like Substances over
638 Tibetan Plateau Due to Long-Range Transported Biomass Burning Emissions, Environ
639 Sci Technol, 53, 14222-14232, 10.1021/acs.est.9b06152, 2019a.
640 Wang, Y., Hu, M., Wang, Y., Zheng, J., Shang, D., Yang, Y., Liu, Y., Li, X., Tang, R.,
641 Zhu, W., Du, Z., Wu, Y., Guo, S., Wu, Z., Lou, S., Hallquist, M., and Yu, J. Z.: The
642 formation of nitro-aromatic compounds under high NOx and anthropogenic VOC
643 conditions in urban Beijing, China, Atmospheric Chemistry and Physics, 19,
644 7649-7665, 10.5194/acp-19-7649-2019, 2019b.
645 Wilcox, E. M., Thomas, R. M., Praveen, P. S., Pistone, K., Bender, F. A. M., and
646 Ramanathan, V.: Black carbon solar absorption suppresses turbulence in the
647 atmospheric boundary layer, Proceedings of the National Academy of Sciences, 113,
648 11794-11799, 10.1073/pnas.1525746113, 2016.

649 Wu, Y., Wang, X., Tao, J., Huang, R., Tian, P., Cao, J., Zhang, L., Ho, K. F., Han, Z.,
650 and Zhang, R.: Size distribution and source of black carbon aerosol in urban Beijing
651 during winter haze episodes, Atmos. Chem. Phys., 17, 7965-7975,
652 10.5194/acp-17-7965-2017, 2017.
653 Zhang, F., Wang, Y., Peng, J., Chen, L., Sun, Y., Duan, L., Ge, X., Li, Y., Zhao, J.,
654 Liu, C., Zhang, X., Zhang, G., Pan, Y., Wang, Y., Zhang, A. L., Ji, Y., Wang, G., Hu,
655 M., Molina, M. J., and Zhang, R.: An unexpected catalyst dominates formation and
656 radiative forcing of regional haze, Proceedings of the National Academy of Sciences,
657 117, 3960-3966, 10.1073/pnas.1919343117, 2020.
658 Zhang, R., Khalizov, A. F., Pagels, J., Zhang, D., Xue, H., and McMurry, P. H.:
659 Variability in morphology, hygroscopicity, and optical properties of soot aerosols
660 during atmospheric processing, Proceedings of the National Academy of Sciences of
661 the United States of America, 105, 10291-10296, 10.1073/pnas.0804860105, 2008.
662 Zhang, Y., Zhang, Q., Cheng, Y., Su, H., Li, H., Li, M., Zhang, X., Ding, A., and He,
663 K.: Amplification of light absorption of black carbon associated with air pollution,
664 Atmospheric Chemistry and Physics, 18, 9879-9896, 10.5194/acp-18-9879-2018,
665 2018a.
666 Zhang, Y., Su, H., Ma, N., Li, G., Kecorius, S., Wang, Z., Hu, M., Zhu, T., He, K.,
667 Wiedensohler, A., Zhang, Q., and Cheng, Y.: Sizing of ambient particles from a Single
668 Particle Soot Photometer measurement to retrieve mixing state of Black Carbon at a
669 Regional site of the North China Plain, Journal of Geophysical Research: Atmospheres,
670 123, 12778-12795, doi:10.1029/2018JD028810, 2018b.
671 Zhao, G., Tao, J., Kuang, Y., Shen, C., Yu, Y., and Zhao, C.: Role of black carbon
672 mass size distribution in the direct aerosol radiative forcing, Atmos. Chem. Phys., 19,
673 13175-13188, 10.5194/acp-19-13175-2019, 2019.
674 Zhao, G., Hu, M., Fang, X., Tan, T., Xiao, Y., Du, Z., Zheng, J., Shang, D., Wu, Z.,
675 Guo, S., and Zhao, C.: Larger than expected variation range in the real part of the

refractive index for ambient aerosols in China, Science of The Total Environment, 779, 146443, 10.1016/j.scitotenv.2021.146443, 2021.

Zheng, J., Hu, M., Du, Z., Shang, D., Gong, Z., Qin, Y., Fang, J., Gu, F., Li, M., Peng, J., Li, J., Zhang, Y., Huang, X., He, L., Wu, Y., and Guo, S.: Influence of biomass burning from South Asia at a high-altitude mountain receptor site in China, Atmospheric Chemistry and Physics, 17, 6853-6864, 10.5194/acp-17-6853-2017, 2017.

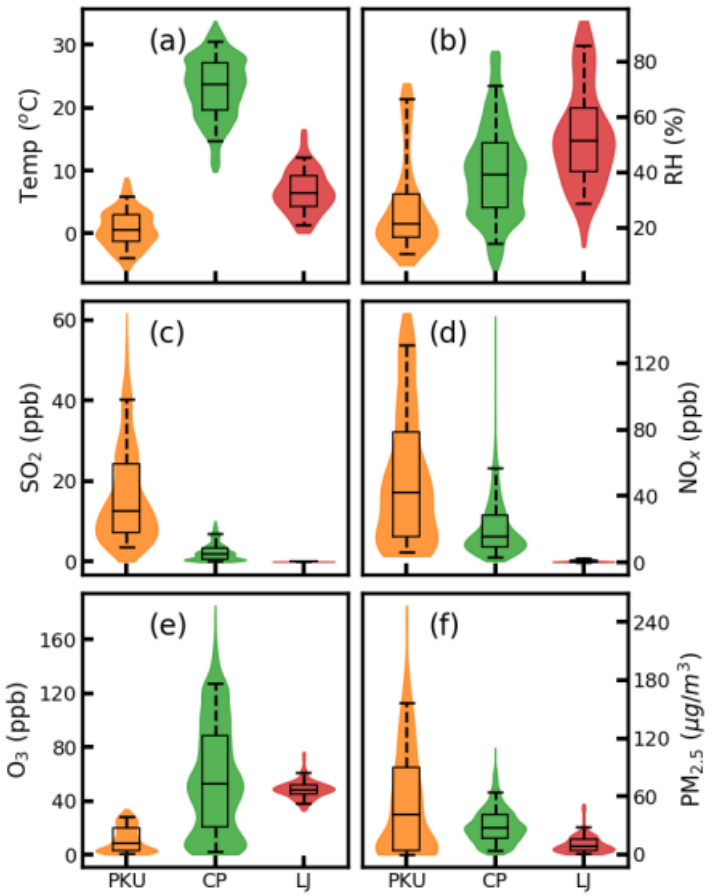

685

686 **Figure 1.** The measured distribution of (a) temperature, (b) RH, (c) SO_2, (d) NOx, (e)
687 O_3 and (f) $PM_{2.5}$ for PKU (orange), CP (green) and LJ (red) sites, respectively. The
688 box and whisker plots represent the 5th, 25th, 75th, and 95th percentiles. The width of
689 the filled colors represents the probability distributions of the corresponding measured
690 values.

691

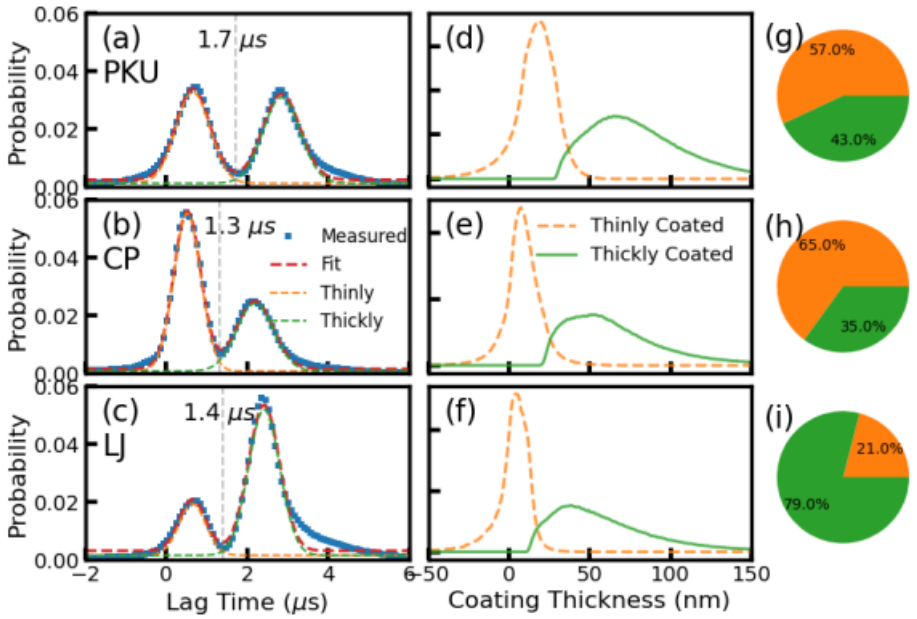

692

693 **Figure 2.** (a) The measured probability distribution of the lag time for the PKU site.
694 Panel (d) shows the corresponding coating thickness distributions of thinly coated
695 (orange) and thickly coated (green) BC-containing aerosols. Panel (g) gives the
696 number fraction of the thinly coated (orange) and thickly coated (green)
697 BC-containing aerosols. Panel (b), (e), and (h) are the corresponding values for the CP
698 site. Panel (c), (f), and (g) give the results for LJ sites.

699

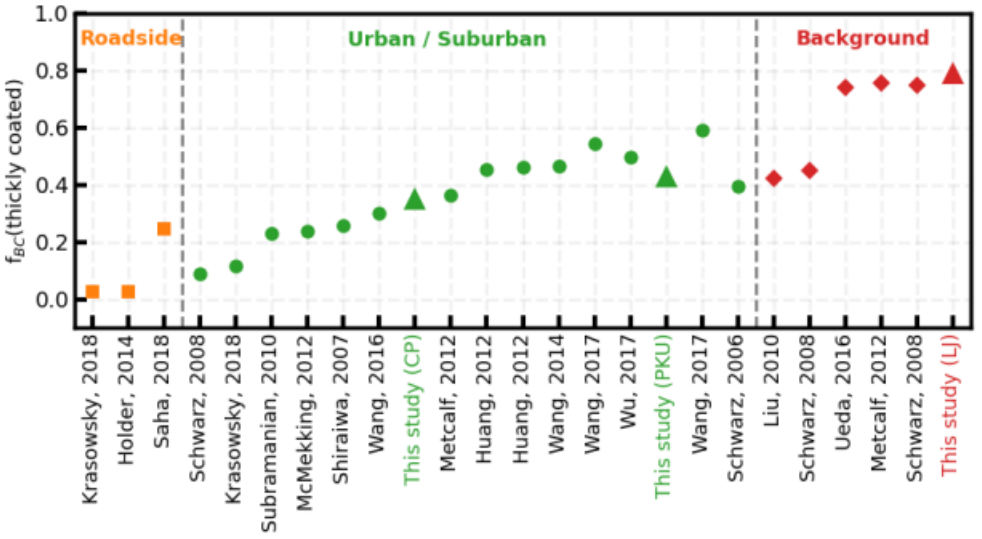

700

701 **Figure 3.** Measured number fraction of the thickly coated BC under different
702 atmospheric environments based on literature. Our measured values are shown as
703 triangles.

704

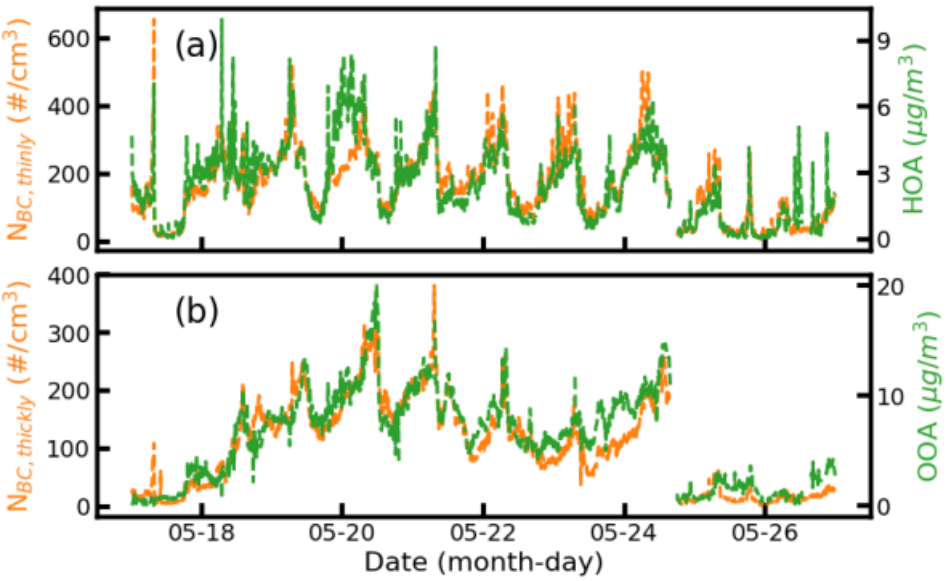

705

706 **Figure 4.** The time series of (a) the number concentration of the thinly coated BC
707 (orange) and the mass concentration of HOA (green), (b) the number concentration of
708 thickly coated BC (orange), and the mass concentration of OOA (green) for the CP
709 site.

710

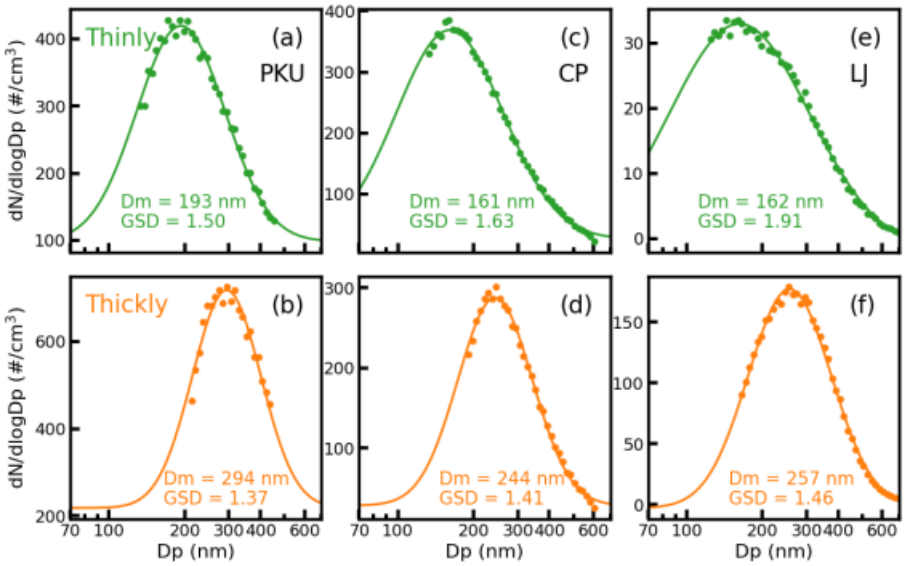

711

712 **Figure 5.** The number size distributions of the thinly coated BC-containing aerosols
713 at (a) PKU, (c) CP, and (e) LJ sites. Panels (b), (d), and (f) are the number size
714 distributions of the thickly coated BC-containing aerosols for the PKU, CP, and LJ
715 sites, respectively. The dots in the figure are the measurement results and the lines are
716 the corresponding fit results with a log-normal distribution.

717

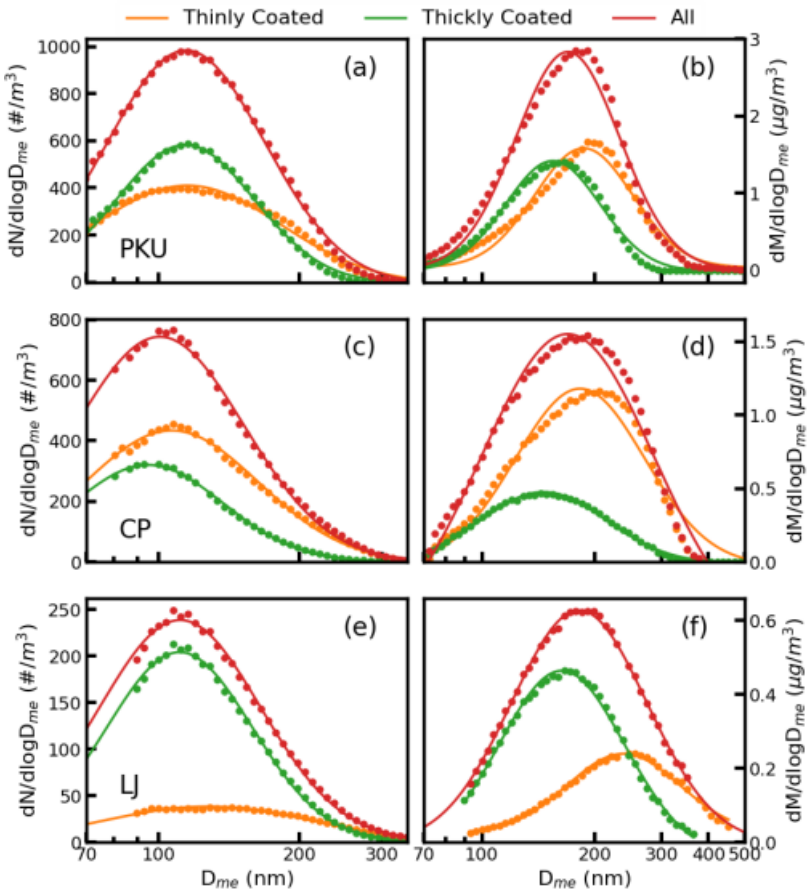

718

719 **Figure 6.** The BC core number size distributions of the thinly coated (orange),
720 thickly coated (green), and overall (red) BC aerosols for the (a) PKU, (c) CP, and (e)
721 LJ sites. Panel (b), (d) (f) show the BC core mass distributions of the thinly coated
722 (orange), thickly coated (orange), and overall (red) BC aerosols for the PKU, CP,
723 and LJ sites, respectively.

724

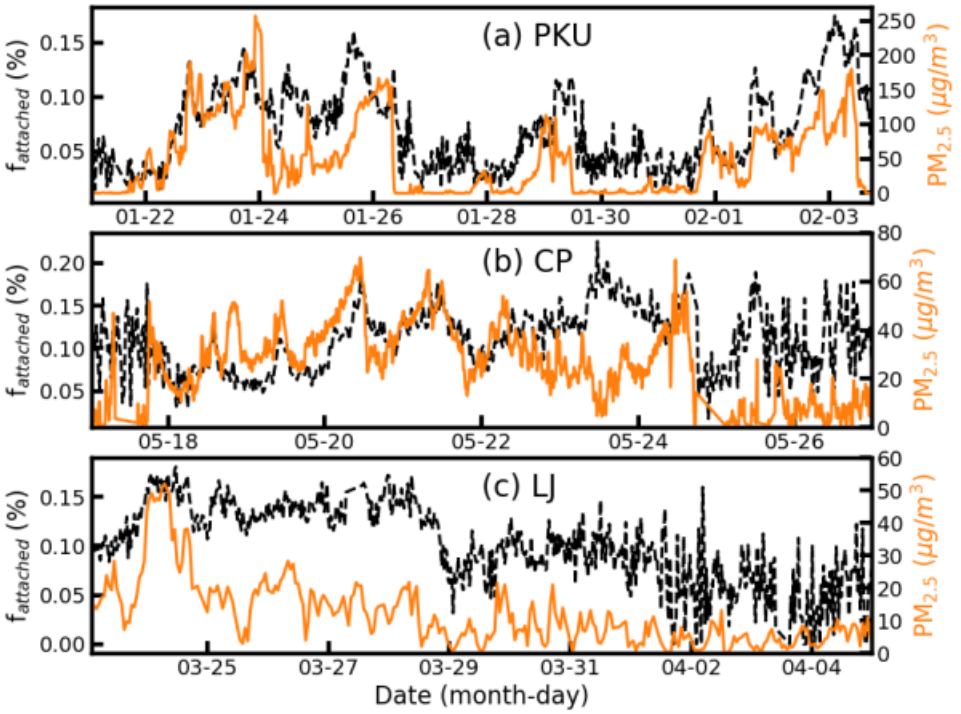

725

726 **Figure 7.** The time series of the number fractions of the attached BC (black) and
727 $PM_{2.5}$ mass concentrations (orange) for the (a) PKU, (b) CP, and (c) LJ sites.

728

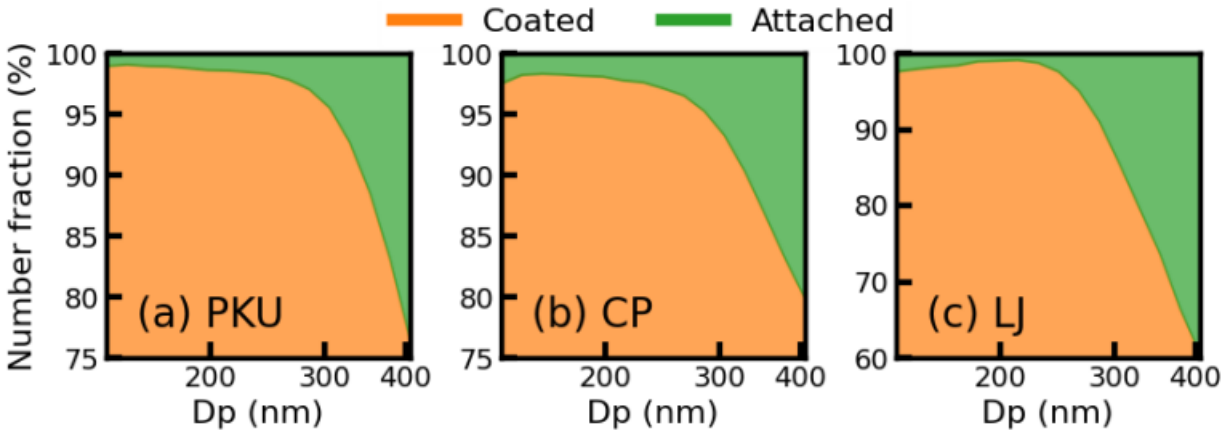

Figure 8. The number fractions of the coated and attached BC under different diameters for the (a) PKU, (b) CP, and (C) LJ sites.

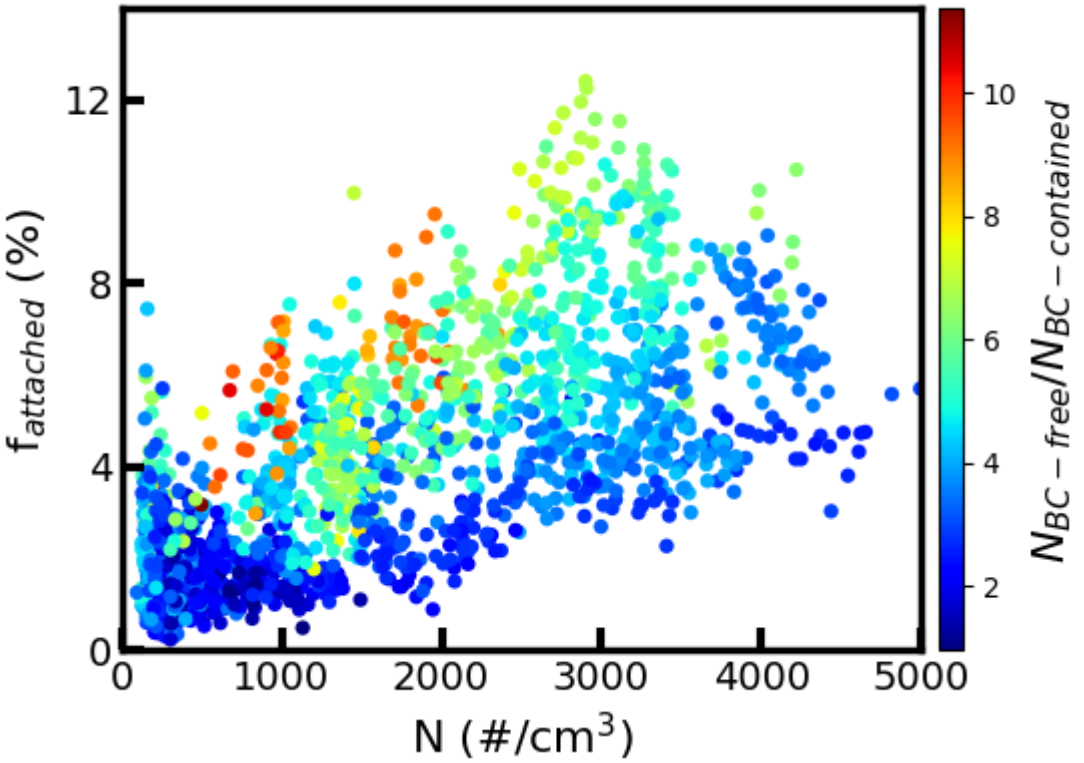

734

735 **Figure 9.** The number fractions of the attached BC aerosols under different total
736 aerosol number concentrations for the CP sites. The filled colors represent the ratios
737 between the BC-fee aerosol number concentrations to the BC-containing aerosol
738 number concentrations.

739

740

741

742

743

744

745

746

747

Table 1. The D_{me} and GSD values of the BC core at different sites.

Site	Value	Number Distribution			Mass Distribution		
		thinly coated	thickly coated	All	thinly coated	thickly coated	All
PKU	D_{me} (nm)	115	114	114	187	154	172
	GSD	1.58	1.40	1.47	1.35	1.34	1.37
CP	D_{me} (nm)	107	95	100	182	146	169
	GSD	1.53	1.45	1.51	1.48	1.47	1.47
LJ	D_{me} (nm)	127	111	112	238	163	181
	GSD	1.68	1.43	1.48	1.47	1.41	1.42